Localized resistance measurements of wrinkled reduced graphene oxide using in-situ transmission electron microscopy

Carbon 113 (2017) 340–345

Contents lists available at ScienceDirect

Carbon

journal homepage: www.elsevier.com/locate/carbon

Localized resistance measurements of wrinkled reduced graphene oxide using *in-situ* transmission electron microscopy

Hanna M. Nilsson [a, b], Ludvig de Knoop [a], John Cumings [b], Eva Olsson [a, *]

[a] Department of Physics, Chalmers University of Technology, 412 96, Gothenburg, Sweden
[b] Department of Material Science and Engineering, University of Maryland, College Park, 20742, MD, USA

ARTICLE INFO

Article history:
Received 25 July 2016
Received in revised form
25 October 2016
Accepted 26 October 2016
Available online 27 October 2016

ABSTRACT

The tunable electrical properties of reduced graphene oxide (rGO) make it an ideal candidate for many applications including energy storage. However, in order to utilize the material for applications it is essential to understand the behavior of the material on the nanoscale, especially how naturally occurring phenomena like wrinkling affect the electronic transport. Here, we use a transmission electron microscope (TEM) with electrical probe *in-situ* holder to perform localized electrical measurements on wrinkled, supported rGO flakes. The TEM allows for observation of the local wrinkled structure of the rGO and simultaneously an electrical probe is used to perform localized resistance measurements. For these measurements, there is no correlation between the electrode distance and the measured resistance indicating that contact resistance varies and dominates the measurements. There is, however, a correlation between increasing number of wrinkles underneath the probe and decreasing resistance, indicating that the wrinkles can provide surface area for contact with the probe and thus lower the resistance. The overall resistance is on the order of single kΩ, if the contact between the probe and the rGO is optimized. These measurements give evidence that rGO with wrinkling can compete as a leading type of graphene for certain applications.

1. Introduction

The reduction of graphene oxide (GO) has been suggested as a route towards both large-scale production of graphene [1] and as a way to tune the electronic properties of the material [2,3]. The most well-studied form of graphene may be chemical vapor deposition (CVD) grown graphene [4], however, despite many years of work, large scale production of graphene using this method does not yet seem economically viable for most applications, thus opening up an opportunity for reduced GO (rGO) to become the material of choice in future electronics and energy storage applications. While graphene is a zero bandgap semiconductor and GO is an insulator, the reduction of GO either by chemical or thermal means, allows for the creation of a material with tunable semimetal or semiconductor properties [5,6]. This makes rGO a promising candidate for applications such as supercapacitors, batteries, and solar cells [7,8]. While theoretical modeling of this material have come a long way in understanding the mechanism of the electron transport as a function of reduction [9,10], less work has been performed measuring the performance of this material in realistic device situations. Thus far there is consensus that the electron mobility of rGO is lower than pristine graphene due to a large amount of sp^3 carbon left from the reduction process [11,12], but some studies suggest that rGO is more robust against extrinsic influences, such as temperature and substrate material [13].

One issue that becomes important when incorporating the material into devices is the formation of wrinkles [14,15]. There have been both theoretical [16] and experimental studies on the effect of wrinkles on the electrical conduction of different types of graphene; GO [17], rGO [18], and pristine, with varied results [19]. Theoretical predictions suggest that wrinkles create additional scattering sites that reduce the electrical conductivity [20], which are confirmed by some localized scanning probe measurements [18,19,21]. However, other measurements of sheets containing wrinkles are inconclusive or point toward no negative influence from wrinkles [15,22,23]. Zhu et al., for example, find that there is anisotropy when looking at the resistance change caused by wrinkles in exfoliated graphene, with measurements along a fold showing lower resistance than control samples without wrinkles,

* Corresponding author.
E-mail address: eva.olsson@chalmers.se (E. Olsson).

http://dx.doi.org/10.1016/j.carbon.2016.10.086

and measurements across a fold showing the same resistance as control samples without wrinkles [22]. Deshpande et al. mapped the Dirac point in chemical vapor deposition (CVD) graphene using scanning tunneling microscopy (STM) and came to the conclusion that there is no correlation between topographical features such as ripples and the electronic structure [23]. A common denominator for many of these measurements is that they either test the entire structure without control of the local structure or they rely only on information obtained from a probe in contact with the graphene. Here, in order to improve the accuracy and control of measurements, we perform transmission electron microscopy (TEM) imaging while simultaneously performing electrical probing measurements. The literature contains limited amount of data for each type of graphene so comparisons must be made between the types rather than within a certain type. However, these comparisons between, for example CVD and rGO, are also valuable as graphitic materials move closer to application ready and choices must be made as to which material is best for each application. We argue that rGO is a better choice than CVD graphene for applications where wrinkles and large contact area ratios are beneficial, such as for catalysts and composite materials. In addition, rGO has more promise in large-scale cost-effective production compared to CVD graphene [8,24].

2. Experimental methods

2.1. Materials preparation

The rGO used in this study was purchased from Angstrom Materials. The product name is "Nano Graphene Platelets." They report ≥95.00 wt% carbon, ≤2.00 wt% hydrogen, ≤0.50 wt% nitrogen, ≤2.50 wt% oxygen, and ≤2.50 wt% ash. The graphene powder is suspended in 1 wt% ammonium laurate (AL) surfactant and is then probe sonicated for 10 min (1 s on/1 s off) at 100 W to disperse the material evenly in solution. This is followed by 15 min of centrifugation at 4000 rpm and decanting the top 50% in order to remove the heavier unwanted particles. The sample membranes used are 50 nm thick SiN TEM windows with 8 Au electrodes. The membranes are plasma cleaned and then left in the rGO solution over night. When they are taken out in the morning they are rinsed with DI water to remove any left over surfactant. The samples are then silver glued (CircuitWorks CW2400) to Au posts so that all of the electrodes can be connected to the bias on a Nanofactory Instruments *in-situ* TEM-STM holder. This glue has a reported resistance of <0.001 Ω-cm. We measure the resistance to be around 2 Ω from the Ag glue to the sample holder.

2.2. Experimental set-up

We employ simultaneous TEM imaging and probe manipulation for optimal control of the local structure during resistance measurements of rGO. The *in-situ* TEM probe holder not only allows us to perform electronic measurements, but it also allows for mechanical manipulation of the structure. Fig. 1 shows an optical microscope image and schematic of the experimental set-up. Silicon nitride membranes with lithographically patterned Au electrodes are used as substrates. rGO flakes are deposited onto the substrates via an ammonium laurate surfactant by leaving the samples in solution overnight [25]. This means that the rGO is simply resting on top of the electrode rather than top-deposited metal, as is common [26]. The sample and a Au tip are then mounted opposite each other in the *in-situ* TEM sample holder (Fig. 1a). The sample's electrode pads are connected to the holder bias using Ag glue and a grounded Au tip is used to probe the sample locally. The TEM that was used is an FEI Tecnai T20 operated at 200 kV with a LaB6 gun.

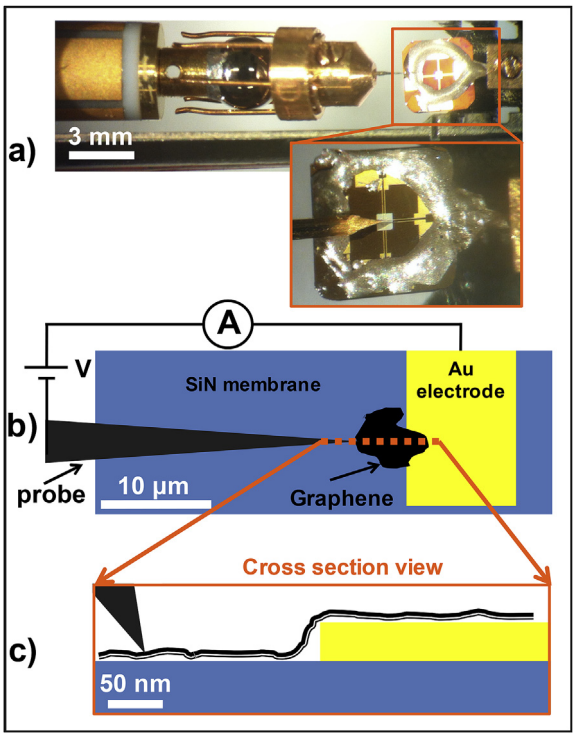

Fig. 1. Experimental set-up. a) Optical microscope image of Nanofactory *in-situ* TEM holder mounted with a patterned SiN membrane and a Au tip. The sample is connected to the holder bias via Ag glue and the Au tip is used to manipulate rGO on the SiN substrate and to perform local electric measurements. b) Top-view schematic of the circuit when the Au tip is used to bias rGO deposited onto Au electrodes. c) Side-view schematic of rGO resting on Au electrodes and SiN substrate while being contacted by a Au probe for electrical and mechanical manipulation.

3. Results and discussion

3.1. Resistance measurements

TEM imaging of these samples allows for locating rGO sheets in contact with Au electrodes and subsequently characterizing their structure. Fig. 2 show a typical TEM image of the rGO that was used in this study. These micron sized flakes were then contacted with the Au probe in multiple different areas for electrical biasing, typically from −1 V to +1 V and then back down to −1 V. Fig. 2 also highlights the method used to estimate the number of wrinkles under the probe at each measurement position. In addition, the distance between the probe and the electrode was recorded for each measurement. The measured total resistance values for this system varies greatly, most are in the 10s of kΩ, which is in accordance with previous literature values for rGO [2,3,27], but some as low as single kΩ and some as high as 100s of kΩs. It would be expected that there would be a correlation between the measured resistance and the distance between the probe and the electrode, but this is not the case here since the contact between the probe and the rGO varies for each measurement. A plot of the resistance as a function of the distance showing that there is no correlation between these two variables is provided in the Supplemental Material in Figs. S1 and S2. The variable that does show correlation to the measured resistance is the number of wrinkles counted under the probe during the measurement, as can be seen in Fig. 3c and will be discussed further below.

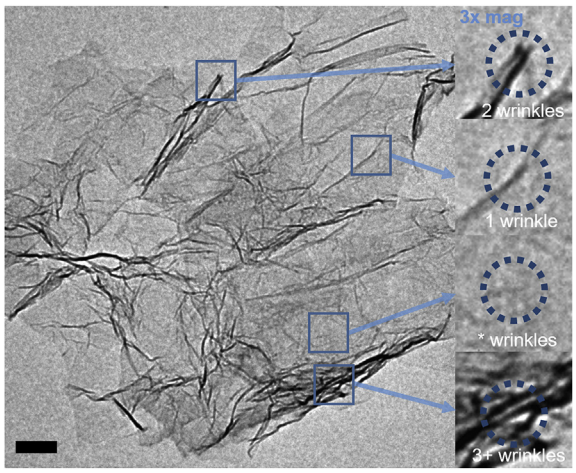

Fig. 2. TEM image of rGO on a SiN membrane. Four difference areas from the TEM image are magnified ×3 on the right and circled with an area approximately the size of the probe contact area in order to show how the number of wrinkles was counted. An asterisk is used to signify areas that do not have a clear wrinkle, but also are not completely flat. When the data is plotted, these textured areas are placed between 0 and 1 wrinkle. The scale bar represents 200 nm.

3.2. Structural and thermal characterization

Raman measurements were performed to characterize the quality of the material. This rGO is reported by the manufacturer to contain 1, 2, and 3 layered sheets of graphene with less than 2.50 wt % oxygen indicating a high level of reduction [28]. The Raman data shown in Fig. 3a is characteristic of few-layered-rGO, as has been described in detail in other studies [1,29,30]. The flakes that have been deposited for these experiments have lateral dimensions ranging from about 0.5 to 3 μm with an aspect ratio of approximately one. Part b) of Fig. 3 shows the resistance change of the rGO throughout a ramp up and ramp down of the applied voltage. Thermal characterization of this system using a technique described elsewhere [31], shows that the temperature of the samples reaches about 200 °C when we apply 1 V of bias to the system, meaning that we can see some effect of the temperature coefficient of resistivity (TCR) of rGO in our measurements. Sun et al. have shown that due to the TCR, the resistance can decrease by as much as 15% when the temperature is increased from 30 to 80 °C, thus we attribute the symmetric decrease in resistance (around 8%) that we see at higher bias in Fig. 3b to heating in the rGO. There is also a 4% decrease in resistance from the ramp up to the ramp down, this can be attributed to annealing of the contact between the rGO and the probe at higher bias [32].

3.3. Contact resistance characterization

Understanding the nature of the contact between graphene and metal pads is an important aspect of graphene electronics. In our tested system we have two types of contacts; (1) graphene resting on top of large Au electrodes and (2) a small Au probe pushing down on the graphene. The contact between graphene and metal pads has been studied extensively [33,34]. Metal deposition on top of graphene is the most common, even though it can introduce doping and change the band structure [35]. However, the most common problem with these types of contacts for electronic applications is that resist is required in the fabrication process, which is difficult to remove without causing damage to the graphene [34]. Resist residue and damage to the graphene from attempts to clean

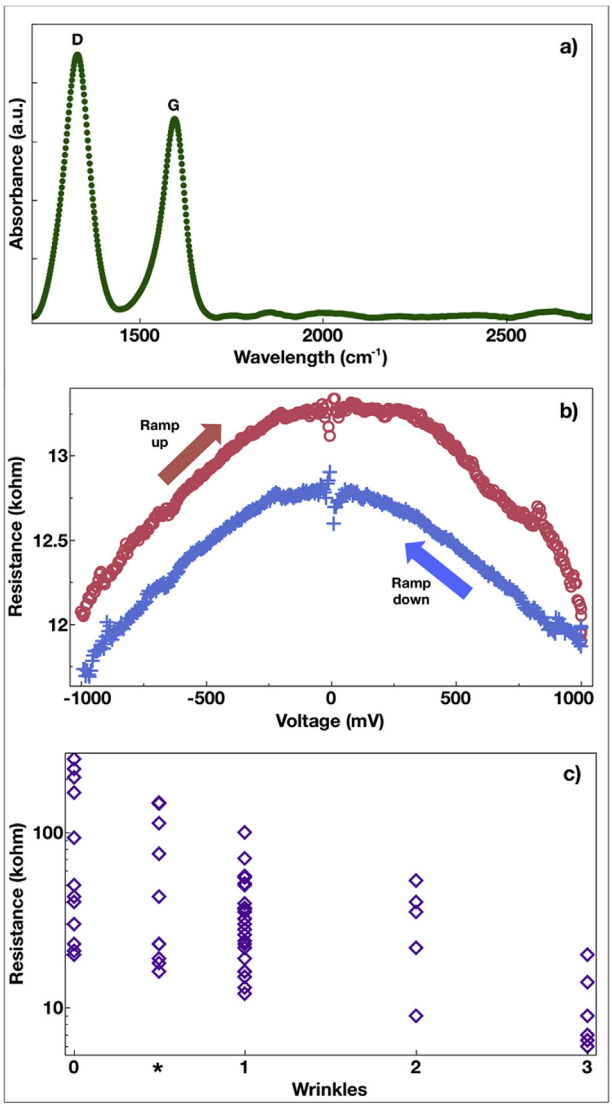

Fig. 3. a) Raman spectra of the tested material showing typical rGO pattern. b) IV data of the rGO showing that the resistance decreases throughout a measurement as a result of thermal annealing of the contact. c) Plot of overall measured resistance as a function of amount of wrinkles in the probe contact area. The * on the x-axis represent test areas with some texture, but no full wrinkle.

the residue, are likely reasons that graphene shows lower contact resistance when bottom-contacts are compared to contacts patterned on top [33]. In addition, in these experiments where the aim is to characterize the original material, it is better to avoid metal deposition that may alter the properties of the graphene. The limiting contact resistance along the current path is caused by the Au probe-graphene since the surface area of the contact area here is several orders of magnitude smaller compared to the contact area between the graphene and the patterned Au electrodes. There is also resistance in the Ag glue that is used to fix the sample to the holder. We have measured this separately to be 2 Ω so we can be sure that it does not affect the data in Figs. 3 and 4. The Ag glue resistance is several orders of magnitude lower than the resistance through the entire sample. This knowledge allows us to place an upper bound on the contact resistivity of the system. If we look at the lowest measured resistance in Fig. 3c for a case without wrinkles (20 kΩ), where we can be sure that the contact area between

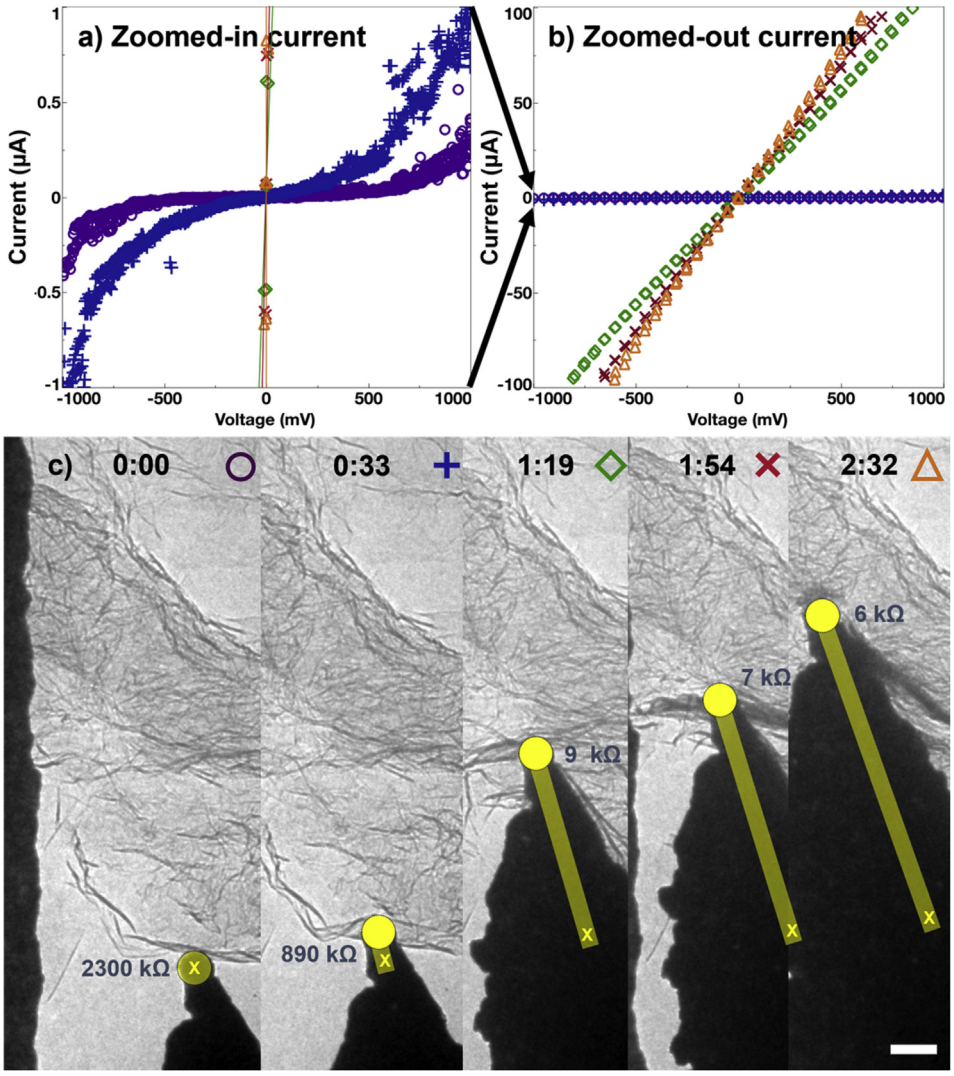

Fig. 4. *In-situ* TEM series of resistance measurements while mechanically manipulating the rGO. a) and b) shows IV data corresponding to the images in c). a) and b) show the same data, but in a) the current axis is scaled to emphasize the first two measurements in c) and b) is scaled to emphasize the last three measurements in c). The resistance decreases as the probe makes more contact with the rGO. The first two measurements show non-linear IV characteristics indicating the influence of contact resistance, but as the probe is dragged along the substrate and makes more contact with the rGO the resistance decreases and becomes almost constant. The time evolution of the probing is given at the top of each frame in c) as min:sec. Scale bar represents 200 nm.

the rGO and a probe with a diameter of 100 nm, then we can say that the contact resistivity is no larger than 2×10^{-6} Ωcm^2. Yan et al., previously found that rGO has at most a contact resistivity of 6.3×10^{-7} Ωcm^2 with top contacted Au [27]. Similar values have been found for top contacted epitaxially grown graphene [34]. Thermal annealing has been shown to be an efficient method to lower contact resistance [33]. As was discussed earlier, we also see this reduction in resistance from annealing of the contact point during measurements.

Here we have a graphene system with both wrinkling and multilayering, which can both play a role in the discussion on contact resistance. It has previously been shown that contact resistance is less of a bottleneck for multilayered systems, lowering the contact resistance of otherwise identical systems in half [33]. Here we are unable to determine the exact number of layers at each measured point, but we note correlation between the wrinkles and the measured resistance without separating out the influence of the number of layers, supporting the significance of dominant contact resistance over bulk sheet resistance. The effect of wrinkles will be divided further into two parts—first we consider the effect on contact resistance, and second we consider the effect on sheet resistance and local potential drops. Fig. 3c shows that the overall measured resistance is lower when measurements are performed on areas with larger amounts of wrinkles underneath the probe. The wrinkles are counted based off of what is visible from TEM images in the area underneath the probe, as shown in Fig. 2. Additionally, in some areas there is visible texture under the probe area, but no full wrinkle; we have included these on the plot between 0 and 1 wrinkle. Due to the uncertainty in the exact contact point between the probe and the rGO in areas with large amounts of wrinkling we choose to group all measurements of this kind in a category of "3 + wrinkles" in order to improve the accuracy of the analysis. However, since the probe is only 100 nm in diameter we never expect that it has the opportunity to contact more than 5 wrinkles during any one measurement. We attribute the correlation of lower measured total resistance with increasing number of wrinkles to the wrinkles increasing the specific contact area between the probe and the graphene. In order to explore this further

we perform a series of measurements where we induce further wrinkling and thus increase the contact between the graphene and the probe. The *in-situ* series of TEM images in Fig. 4 shows the probe initially placed on the SiN at the bottom of the rGO sheet and then subsequently pushed along the SiN membrane up against the graphene, introducing more wrinkles. The IV plots in Fig. 4a) and b) show that the resistance values decrease drastically at first and then level off. Note that the current is scaled drastically different for 4a) and 4b) to be able to emphasize the behaviors at different resistance levels. Initially, the IV characteristics are highly non-linear showing that contact resistance is dominant, but as the contact improves the resistance decreases and the IV curves become almost perfectly linear. In this example, the resistance decreases to 6 kΩ, which as will be discussed in the next section, is a reasonable value for the sheet resistance, without any contact resistance.

3.4. Sheet resistance calculations

Sheet resistance is an important figure of merit for graphene. For sheet resistance values in the literature, studies also point to bi-layered systems having higher electrical conduction capabilities than single layered graphene [11,36]. This is attributed to monolayer graphene being more sensitive to strain and substrate interactions. Other measurements on rGO report sheet resistances from about 2 to 50 kΩ/sq. [2,3,27]. These values are higher than those reported for CVD grown graphene, which are typically an order of magnitude lower [26,33,37]. However, the advantages in ease of fabrication of rGO and for certain applications where large contact area is advantageous, rGO may be a better option despite a lower sheet resistance. For our measurements we can again place upper bounds on the sheet resistance by saying that for cases where the total measured resistance is lowest, the contact resistance is negligible and all can be attributed as sheet resistance. The aspect ratio of our sheets is approximately 1 so we estimate an upper bound of the sheet resistance as 6 kΩ/sq., which falls in the range of prior reported values. This sheet resistance includes the resistance that could potentially be introduced by potential drops at individual wrinkles, which indicates there is no evidence in our results that the wrinkles cause an increase in the resistance. Similarly, ref. [23] conclude that wrinkles do not cause a shift in the electrochemical potential of exfoliated graphene.

4. Conclusion

By using an *in-situ* TEM technique to characterize and control the local structure of rGO sheets deposited on a substrate, we have been able to characterize electronic properties, including the influence of wrinkles. We find that contact resistance is the dominant factor in the measured values as indicated by the lack of correlation between electrode distance and resistance. We further find that the amount of local wrinkling at the contact between the probe and the rGO correlates to a reduction in the measured resistance, plausibly because larger amounts of wrinkles allow for larger contact areas with the probe. We see a decrease in resistance during measurements caused both by an increase in temperature and by annealing of the contact between the probe and the rGO. Our measurements allow us to place upper bounds on both contact resistivity and sheet resistance of the tested material (2×10^{-6} Ωcm^2 and 6 kΩ/sq., respectively). These values are comparable to previously reported measurements on rGO. Our work supports a conclusion that rGO is an electrically robust material that can perform well on electronic systems even with wrinkles and nanoscale metal contacts. We see that electrical atomic force microscopy measurements would be an interesting continuation of this work that may provide additional insight to the observed phenomenon.

Acknowledgment

This work is supported by Vetenskapsrådet award no. 326-2014-4836, the Knut and Alice Wallenberg Foundation under "The Swedish graphene initiative," the European Network for Electron Microscopy (ESTEEM2, European Union Seventh Framework Program under Grant Agreement 312483-ESTEEM2 (Integrated Infrastructure Initiative–I3)), and partial support from the US Department of Energy, Office of Basic Energy Sciences, Division of Materials Sciences and Engineering award no. DE-FG02-10ER46742. HMN was supported by a National Science Foundation Graduate Research Fellowship (award no. DGE1322106).

Appendix A. Supplementary data

Supplementary data related to this article can be found at http://dx.doi.org/10.1016/j.carbon.2016.10.086.

References

[1] S. Stankovich, D.A. Dikin, R.D. Piner, K.A. Kohlhaas, A. Kleinhammes, Y. Jia, Y. Wu, S.T. Nguyen, R.S. Ruoff, Synthesis of graphene-based nanosheets via chemical reduction of exfoliated graphite oxide, Carbon 45 (7) (2007) 1558–1565.
[2] Z. Wei, D. Wang, S. Kim, S.-Y. Kim, Y. Hu, M.K. Yakes, A.R. Laracuente, Z. Dai, S.R. Marder, C. Berger, W.P. King, W.A. de Heer, P.E. Sheehan, E. Riedo, Nanoscale tunable reduction of graphene oxide for graphene electronics, Science 328 (5984) (2010) 1373–1376.
[3] G. Eda, G. Fanchini, M. Chhowalla, Large-area ultrathin films of reduced graphene oxide as a transparent and flexible electronic material, Nat. Nanotechnol. 3 (5) (2008) 270–274.
[4] J. Sun, N. Lindvall, M.T. Cole, T. Wang, T.J. Booth, P. Boggild, K.B.K. Teo, J. Liu, A. Yurgens, Controllable chemical vapor deposition of large area uniform nanocrystalline graphene directly on silicon dioxide, J. Appl. Phys. 111 (4) (2012).
[5] X. Wu, M. Sprinkle, X. Li, F. Ming, C. Berger, W.A. de Heer, Epitaxial-graphene/graphene-oxide junction: an essential step towards epitaxial graphene electronics, Phys. Rev. Lett. 101 (2) (2008).
[6] I. Jung, D.A. Dikin, R.D. Piner, R.S. Ruoff, Tunable electrical conductivity of individual graphene oxide sheets reduced at "low" temperatures, Nano Lett. 8 (12) (2008) 4283–4287.
[7] K.S. Novoselov, V.I. Fal'ko, L. Colombo, P.R. Gellert, M.G. Schwab, K. Kim, A roadmap for graphene, Nature 490 (7419) (2012) 192–200.
[8] D. Lin, Y. Liu, Z. Liang, H.-W. Lee, J. Sun, H. Wang, K. Yan, J. Xie, Y. Cui, Layered reduced graphene oxide with nanoscale interlayer gaps as a stable host for lithium metal anodes, Nat. Nanotechnol. 11 (2016) 626–632.
[9] M. Lundie, Z. Sljivancanin, S. Tomic, Electronic and optical properties of reduced graphene oxide, J. Mater. Chem. C 3 (29) (2015) 7632–7641.
[10] S. Zhou, A. Bongiorno, Origin of the chemical and kinetic stability of graphene oxide, Sci. Rep. 3 (2013).
[11] C. Gomez-Navarro, R.T. Weitz, A.M. Bittner, M. Scolari, A. Mews, M. Burghard, K. Kern, Electronic transport properties of individual chemically reduced graphene oxide sheets, Nano Lett. 7 (11) (2007) 3499–3503.
[12] G. Eda, C. Mattevi, H. Yamaguchi, H. Kim, M. Chhowalla, Insulator to semimetal transition in graphene oxide, J. Phys. Chem. C 113 (35) (2009) 15768–15771.
[13] R. Lanche, L.E. Delle, M. Weil, V. Xuan Thang, V. Pachauri, W.M. Munief, P. Wagner, S. Ingebrandt, Routine fabrication of reduced graphene oxide microarray devices via all solution processing, Phys. Status Solidi a-Applications Mater. Sci. 210 (5) (2013) 968–974.
[14] H. Zhang, Y. Zhang, B. Wang, Z. Chen, Y. Zhang, Y. Sui, G. Yu, Z. Jin, X. Liu, Stripe distributions of graphene-coated Cu foils and their effects on the reduction of graphene wrinkles, Rsc Adv. 5 (117) (2015) 96587–96592.
[15] N.H. Kim, Y. Ko, S.-R. Cho, S.T. Chang, Formation and characterization of wrinkle structures of chemically-derived graphene thin films and micropatterns, J. Nanosci. Nanotechnol. 14 (5) (2014) 3774–3777.
[16] K. Zhang, M. Arroyo, Understanding and strain-engineering wrinkle networks in supported graphene through simulations, J. Mech. Phys. Solids 72 (2014) 61–74.
[17] L.J. Cote, J. Kim, Z. Zhang, C. Sun, J. Huang, Tunable assembly of graphene oxide surfactant sheets: wrinkles, overlaps and impacts on thin film properties, Soft Matter 6 (24) (2010) 6096–6101.
[18] S. Ladak, J.M. Ball, D. Moseley, G. Eda, W.R. Branford, M. Chhowalla, T.D. Anthopoulos, L.F. Cohen, Observation of wrinkle induced potential drops in biased chemically derived graphene thin film networks, Carbon 64 (2013) 35–44.

[19] K. Xu, P. Cao, J.R. Heath, Scanning tunneling microscopy characterization of the electrical properties of wrinkles in exfoliated graphene monolayers, Nano Lett. 9 (12) (2009) 4446–4451.
[20] F. Guinea, B. Horovitz, P. Le Doussal, Gauge fields, ripples and wrinkles in graphene layers, Solid State Commun. 149 (27–28) (2009) 1140–1143.
[21] A.L. Vazquez de Parga, F. Calleja, B. Borca, M.C.G. Passeggi Jr., J.J. Hinarejos, F. Guinea, R. Miranda, Periodically rippled graphene: growth and spatially resolved electronic structure, Phys. Rev. Lett. 100 (5) (2008).
[22] W. Zhu, T. Low, V. Perebeinos, A.A. Bol, Y. Zhu, H. Yan, J. Tersoff, P. Avouris, Structure and electronic transport in graphene wrinkles, Nano Lett. 12 (7) (2012) 3431–3436.
[23] A. Deshpande, W. Bao, Z. Zhao, C.N. Lau, B.J. LeRoy, Spatial mapping of the dirac point in monolayer and bilayer graphene, Ieee Trans. Nanotechnol. 10 (1) (2011) 88–91.
[24] M. Fathy, A. Gomaa, F.A. Taher, M.M. El-Fass, A.E.-H.B. Kashyout, Optimizing the preparation parameters of GO and rGO for large-scale production, J. Mater. Sci. 51 (12) (2016) 5664–5675.
[25] H.M. Nilsson, B. Meany, J. Ticey, C.-F. Sun, Y. Wang, J. Cumings, Ammonium laurate surfactant for cleaner deposition of carbon nanotubes, Langmuir 31 (25) (2015) 6948–6955.
[26] K. Asadi, E.C. Timmering, T.C.T. Geuns, A. Pesquera, A. Centeno, A. Zurutuza, J.H. Klootwijk, P.W.M. Blom, D.M. de Leeuw, Up-scaling graphene electronics by reproducible metal-graphene contacts, Acs Appl. Mater. Interfaces 7 (18) (2015) 9429–9435.
[27] L. Yan, C. Punckt, I.A. Aksay, W. Mertin, G. Bacher, Local voltage drop in a single functionalized graphene sheet characterized by kelvin probe force microscopy, Nano Lett. 11 (9) (2011) 3543–3549.
[28] C. Mattevi, G. Eda, S. Agnoli, S. Miller, K.A. Mkhoyan, O. Celik, D. Mastrogiovanni, G. Granozzi, E. Garfunkel, M. Chhowalla, Evolution of electrical, chemical, and structural properties of transparent and conducting chemically derived graphene thin films, Adv. Funct. Mater. 19 (16) (2009) 2577–2583.
[29] K.N. Kudin, B. Ozbas, H.C. Schniepp, R.K. Prud'homme, I.A. Aksay, R. Car, Raman spectra of graphite oxide and functionalized graphene sheets, Nano Lett. 8 (1) (2008) 36–41.
[30] D. Yang, A. Velamakanni, G. Bozoklu, S. Park, M. Stoller, R.D. Piner, S. Stankovich, I. Jung, D.A. Field, C.A. Ventrice Jr., R.S. Ruoff, Chemical analysis of graphene oxide films after heat and chemical treatments by X-ray photoelectron and Micro-Raman spectroscopy, Carbon 47 (1) (2009) 145–152.
[31] T. Brintlinger, Y. Qi, K. Baloch, D. Goldhaber-Gordon, J. Cumings, Electron thermal microscopy, Nano Lett. 8 (2) (2008) 582–585.
[32] P. Sun, M. Zhu, K. Wang, M. Zhong, J. Wei, D. Wu, H. Zhu, Small temperature coefficient of resistivity of graphene/graphene oxide hybrid membranes, Acs Appl. Mater. Interfaces 5 (19) (2013) 9563–9571.
[33] A.V. Babichev, V.E. Gasumyants, A.Y. Egorov, S. Vitusevich, M. Tchernycheva, Contact properties to CVD-graphene on GaAs substrates for optoelectronic applications, Nanotechnology 25 (33) (2014).
[34] J.A. Robinson, M. LaBella, M. Zhu, M. Hollander, R. Kasarda, Z. Hughes, K. Trumbull, R. Cavalero, D. Snyder, Contacting graphene, Appl. Phys. Lett. 98 (5) (2011).
[35] C. Gong, D. Hinojos, W. Wang, N. Nijem, B. Shan, R.M. Wallace, K. Cho, Y.J. Chabal, Metal-graphene-metal sandwich contacts for enhanced interface bonding and work function control, Acs Nano 6 (6) (2012) 5381–5387.
[36] M.M. Benameur, F. Gargiulo, S. Manzeli, G. Autes, M. Tosun, O.V. Yazyev, A. Kis, Electromechanical oscillations in bilayer graphene, Nat. Commun. 6 (2015).
[37] A.V. Babichev, S.A. Rykov, M. Tchernycheva, A.N. Smirnov, V.Y. Davydov, Y.A. Kumzerov, V.Y. Butko, Influence of substrate microstructure on the transport properties of CVD-graphene, Acs Appl. Mater. Interfaces 8 (1) (2016) 240–246.